

An Automated Design Tool for Three-phase Motor Drives

Zhou Dong
Min H. Kao Dept. of EECS
The University of Tennessee
Knoxville, USA
zdong9@vols.utk.edu

Ren Ren
Monolithic Power System,
Inc.
San Jose, USA
rren3@vols.utk.edu

Fred Wang
Min H. Kao Dept. of EECS
Oak Ridge National Lab
The University of Tennessee
Knoxville, USA
fred.wang@utk.edu

Ruirui Chen
Min H. Kao Dept. of EECS
The University of Tennessee
Knoxville, USA
rchen14@vols.utk.edu

Abstract—This paper presents an automated design tool for three-phase motor drives. The design tool integrates state-of-the-art design algorithms and component models to reduce paper design efforts for engineers. The converter is optimized for minimum weight considering comprehensive design constraints and conditions configured by users. The software is modular so that some component models can be selected by users based on design speed and accuracy considerations. The user interface (UI) of the tool is developed with the App designer, and both the design algorithms and models are implemented by M-script in MATLAB. Besides, eight databases for components, including devices, passives, and cooling, are built with commercially available products and can be managed by users. The final design results can be visualized in detail. A case study is presented to show how the design tool works.

Keywords—design tool, motor drive, design automation

I. INTRODUCTION

The three-phase motor drive design incorporates device selection, thermal management system (TMS) design, filter design, and bus capacitor selection as an example shown in Fig. 1. Due to couplings between different domains, iterations are normally required for the design and optimization, which is time-consuming with a tremendous number of design variables [1]-[3]. Moreover, with emerging applications, like electrified transportations, engineers need to design and optimize the motor drive under various design specifications, e.g., input voltage, to optimize the system. This would require massive efforts if designing and optimizing them manually. To save the design time and efforts, an automated design tool is desired for the three-phase motor drive.

The challenges of developing a comprehensive design tool for a three-phase motor drive include 1) various design variables for the complex system; 2) the trade-off between model accuracy and computational efforts; 3) the discrete optimization for the non-deterministic polynomial-time (NP) hard problem; 4) fast simulation speed to get accurate waveforms; 5) the database management for a huge number of components; 6) adapting for different design objectives. There are very limited comprehensive design tools developed

due to these challenges. Ref [4]-[6] represented some early attempts with relatively limited scope, integration, and availability. There is also one commercial software PowerForge [7], however without much published or shared information on its models and design algorithms. Given the continued advances and needs in motor drives, it should be valuable to share the design tool developed by the authors and their colleagues with clearly described models and design algorithms.

This paper presents a comprehensive design tool integrating state-of-the-art design algorithms and models for the three-phase motor drive design to dramatically reduce the paper design efforts for users. It is a result of the effort by the authors and their colleagues for the last 10 years. The design tool enables weight optimization and shrinks the gaps between the paper design and hardware prototype. All the design algorithms and models utilized are presented for users' information. Moreover, the software is modular so that models can be replaced based on users' favor.

II. DESIGN TOOL FUNCTION AND ARCHITECTURE

A. Design Tool Function

The design tool is mainly for the weight optimization of the motor drive assuming the electrified aircraft propulsion application. It can be extended to other objectives for different applications. Several commonly used topologies and PWM modulation schemes are included in the software as listed in TABLE I. Users can select one of them or compare them for the optimal design case.

TABLE I. TOPOLOGIES AND PWM MODULATIONS SCHEMES AVAILABLE FOR THE DESIGN TOOL

Topologies	Modulation schemes
2-level	SVPWM, DPWM
3-level ANPC	SVPWM, DPWM, CMR
3-level T-type	SVPWM, DPWM, CMR
Multi-level flying capacitor clamping	Phase shift, level shift
Multi-level diode clamping	Phase shift, level shift

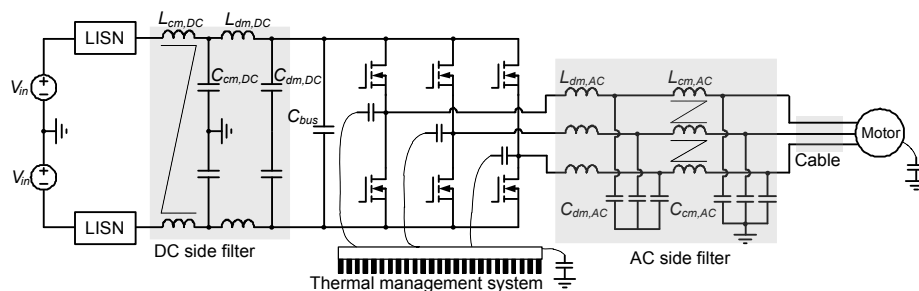


Fig. 1 Three-phase motor drive system with an example of two-level converter

The optimization of the motor drive design is formalized as selecting design variables based on design constraints, conditions, and objectives [8]. The formulation of the design optimization is shown in Fig. 2. Design conditions include the source, load, and environmental conditions specified for the design. Design constraints are either the system level constraints, like the efficiency, EMI, and THD requirements, or the physical limits of devices and passive components. For EMI and THD constraints, options in the tool include DO-160 E and MIL-461. Design variables are what the design tool tries to select for the optimal design objective.

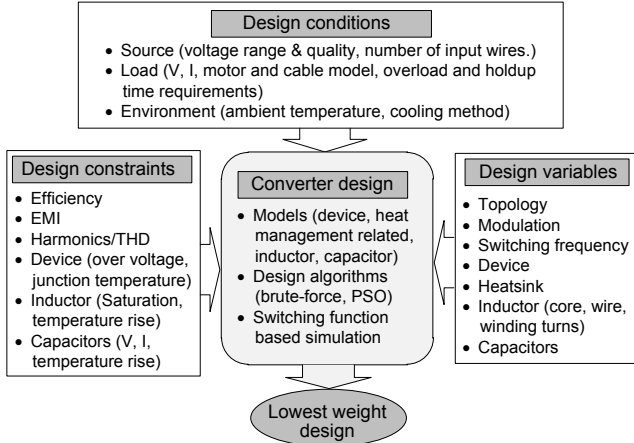


Fig. 2 Formulation of converter design optimization

B. Design Tool Architecture

The database, component models, design algorithms, and simulation are four critical aspects of the design tool architecture as shown in Fig. 3. The database provides the information from datasheets of components (devices, passives, and cooling components, etc.). Modeling covers required models for electrical, thermal, and mechanical designs. Models are mainly analytical to minimize the need to use simulation software like FEM simulation software. This can avoid the issues with long simulation time and possible issues with interfaces when a certain commercial simulation software is updated. Design algorithms are conducted to

minimize the design time for the optimal design result based on component models and design requirements. Simulation is used to get the waveforms for the design. The details of these four aspects are introduced in the following sections.

III. DESIGN ALGORITHMS AND SWITCHING-FUNCTION-BASED SIMULATION

The design algorithms can be separated into the system-level and converter-level ones.

A. System-level Design Algorithm

For system-level optimization, the design tool enables the evaluation of different topologies, PWM modulation schemes, switching frequencies, filter configurations (single-stage or two-stage, LC or CL structure), and cooling methods (passive or active, air or liquid cooling) as shown in Fig. 4. For each combined configuration, the converter-level design is implemented firstly to output an optimal design result for the design result pool. Then, iterations are conducted with different combined configurations. Finally, the design result pool includes optimal designs for each configuration. By comparing the designs in the design result pool, the best configuration with the optimized design result can be picked.

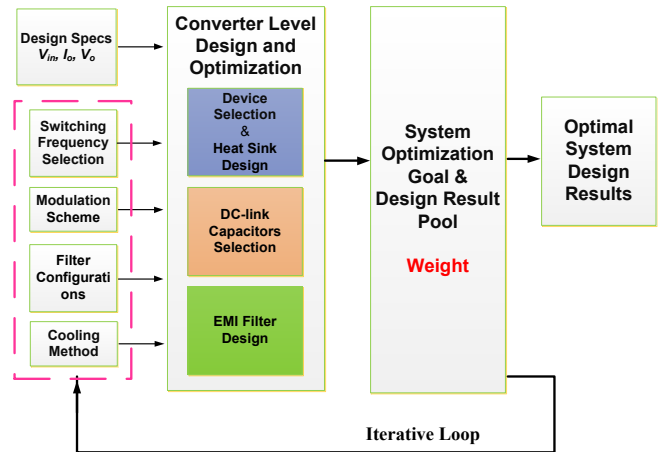


Fig. 4. System-level optimization

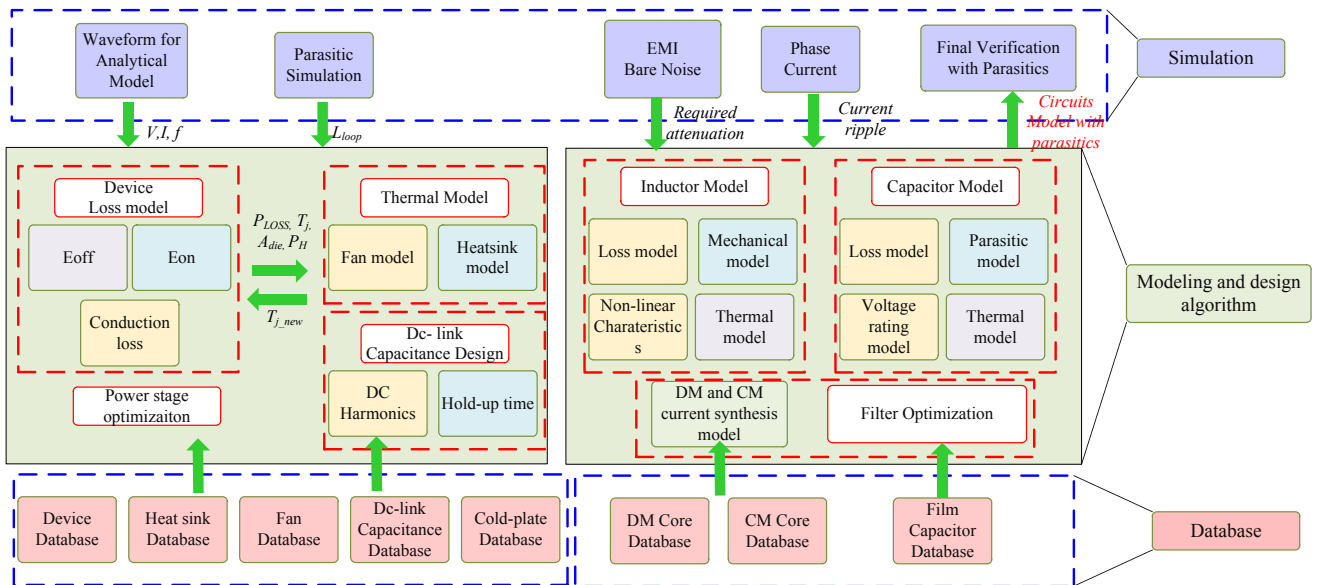


Fig. 3. Architecture of the design tool

B. Converter-level Design Algorithm

For a specific case with the determined configuration, the design is conducted for the weight optimization by selecting different devices, passives, and cooling components. The design sequence is 1) DC-link capacitors selection, 2) Devices selection and TMS design, and 3) filter design.

The design first starts with the selection of DC-link capacitors. The capacitance is determined by the bus voltage ripple and hold-up time requirements. The simulated input current waveforms of the converter are used, which would not be influenced by device and filter selections. The design flow is shown in Fig. 5. After the determination of the capacitance, the physical selection of capacitors can be done by brute-force searching of the capacitors in the database for the minimum weight combination.

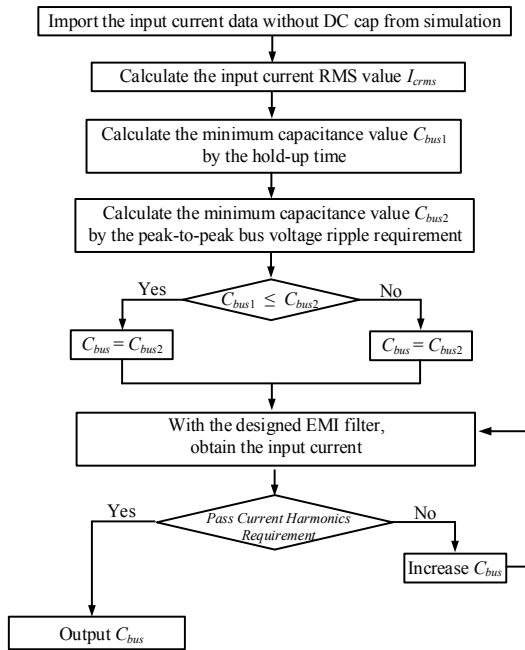


Fig. 5. DC-link capacitance determination

For the device selection and TMS design, the flow chart is shown in Fig. 6 with an example of the forced air cooling. Devices are first selected to meet the voltage and current requirements. Normally, many device combinations are qualified. For each qualified device combination, the power loss is calculated based on the simulation waveforms. Then, based on the power loss, surface area, and maximum junction temperature requirements of the devices, the TMS can be designed and optimized for each case. By comparing these qualified combinations of devices and TMSs, the one with the minimum weight is selected.

Filters in the three-phase motor drive may include the DC side EMI filter and AC side EMI filter or AC side dv/dt filter depending on the system requirements. For EMI filters, DM (differential mode) and CM (common mode) filters are coupled because leakage inductance of CM inductor can function as the whole or part of the DM inductance. This increases the combination number of inductors and capacitors as input variables for optimization. The particle swarm optimization (PSO) [9] is adopted to reduce the searching efforts of different combinations of LC values in the filter.

Take the design and optimization of a single-stage EMI filter as an example in Fig. 7. To get an optimal design for the LC value determination, with required DM and CM corner frequencies from the bare noise analysis, two design variables C_{cm} and k (inductance ratio between DM inductance and CM inductance) need to be iterated to consider the coupling to achieve the lowest weight. PSO is then used to optimize the two design variables. For each LC combination, physical designs of inductors and capacitors are conducted with the simulated waveforms. It can be optimized by the brute-force search of the core and number of turns, and capacitors for the minimum weight.

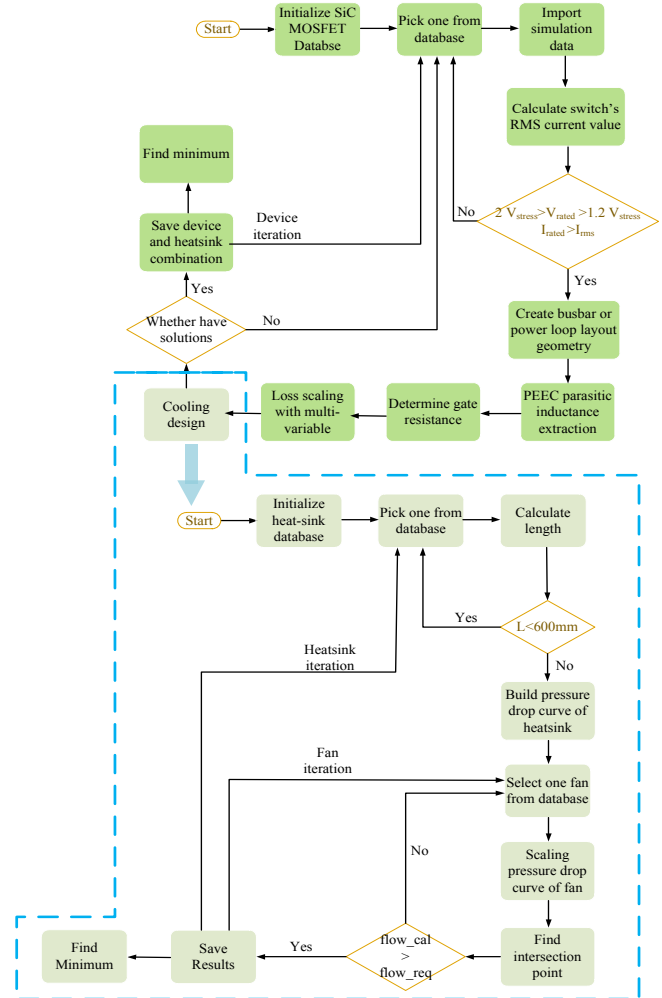


Fig. 6. Design flow of devices and TMS

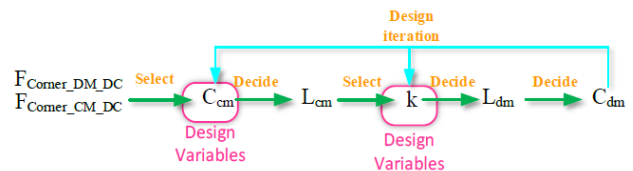


Fig. 7. Design flow of single-stage EMI filter

C. Switching-function-based Simulation

For each design step discussed above, simulation waveforms are always required. This means the simulation needs to be repeated many times for a single case design. Therefore, the simulation speed is critical for the overall design speed.

Switching-function-based simulations are adopted to replace the conventional switch-based simulation in the tool [10]. Although the edge of the real switching actions would not be considered, the influence on design results is minor because the sharp switching edges of the PWM voltage have been verified to have very limited influence on the design [11].

IV. DEVICE AND COMPONENT MODELS

It can be noted that in Section III, devices and components models are utilized to evaluate the design performance. In this section, all models in the tool are given in detail.

There are two types of design routines available for the design tool: fast and advanced design routines. The main difference is the models used in the design. The fast design routine utilizes simple models to minimize the design time. The advanced design routing considers some nonlinear characteristics to minimize the gap between the paper design and prototyping. Detailed models are listed in TABLE II. The selectable design routines benefit from the modular structure of the software. Models can be individually improved and updated by tool developers and even users once the software is open source.

A. Device Models

Power device modeling is mainly about the loss model and thermal model. For the fast routine, these model-related parameters, including R_{dson} at different temperatures, E_{on} and E_{off} at a certain voltage and current stress, and thermal resistance, are obtained from the database. R_{dson} is determined by the maximum junction temperature set by users. E_{on} and E_{off} are scaled by voltage and current stress in the simulation.

The drawback of this model is that E_{on} and E_{off} from the datasheet are based on tests with specific gate resistances and layouts of the commutation loop, which is very likely to be different in the final prototyping. Therefore, for the advanced design routine, the discrete-time modeling of switching behavior is applied to predict the switching behavior and loss considering more input variables [12]. With the advanced models, the gate resistance is optimized to meet both the temperature and voltage constraints considering the parasitic

inductance of the pre-defined power loop extracted with the partial element equivalent circuits (PEEC) method [13]. As for the device thermal model, both routines utilized R_{th} from the datasheet.

B. TMS Related Models

The forced air cooling and liquid cooling are two options integrated into the software. For the forced air cooling with fans and extruded heatsinks, three correction factors, including the length of heatsinks, the temperature of heatsinks, and airflow velocity, are considered for thermal resistance determination of extruded heatsinks based on [14]. The pressure drops of the fans and heatsinks are also considered by the model in [15] to select the fan and determine the airflow velocity. Cold plate thermal resistance is determined by the flow rate based on their relationship pre-stored in the database. Besides, the thermal resistance of the thermal grease is also considered with the thermal conductivity, thickness, and area.

C. Magnetics Models

For magnetics, powdered iron and amorphous alloy cores with a distributed air gap structure are mainly considered in the design. For fast routine, the inductance per single turn squared A_L provided by manufacturers is used to estimate the inductance [16]. Then the magnetic flux density B is calculated with $B = \mu \frac{NI}{l}$ to check whether it exceeds the saturation range of magnetic cores. The leakage inductance models of common-mode chokes used are from [17]-[18].

For the advanced routine, the impact of the current-bias dependent permeability is considered for the DC inductance modeling [19], which can induce unbalanced DM impedances due to unequal three-phase instantaneous currents to worsen EMI noises. Besides, the impedance-based design approach considering both the frequency-dependent and imaginary permeability of nanocrystalline cores is used for a more accurate design [20].

For both routines, the core loss is calculated with iGSE considering the trade-off of accuracy and computational efforts [21]. For the winding loss, DC and AC loss are decoupled. DC loss is determined by the copper DC resistance at the operating temperature. AC loss considers the proximity

TABLE II. MAIN DEVICE AND COMPONENT MODELS USED IN THE DESIGN TOOL

Category	Models	Fast design routine	Advanced design routine
Device models	Conduction loss	R_{dson} at maximum junction temperatures set by users	
	Switching loss	Scaled E_{on} and E_{off} with voltage and current stress	Discrete-time modeling with parasitic, device nonlinear characteristics, and R_g [12]
TMS related models	Forced or natural air thermal resistance	Correction factors including airflow velocity, heatsink length, and temperature rise [14]	
	Fan model	Airflow velocity determined by pressure drops of the fans and heatsinks [15]	
	Liquid cooling thermal resistance	Cold plate thermal resistance determined by flow rate based on datasheet	
Magnetics models	Inductance model	Inductance per single turn squared A_L provided by manufacturers [16]	Consider current-bias dependent permeability [19] and frequency-dependent imaginary permeability [20]
	Leakage inductance model	Leakage inductance model of common mode choke from [17]-[18]	
	Core loss model	iGSE [21]	
	Winding loss model	Sum up separated losses at different frequencies based on FFT analysis of current [22]	
	Thermal model	Level 2 thermal model [23]	
Capacitor models	Impedance model	Series LRC circuit with ESL and ESR [24]	
	Thermal model	Thermal resistance provided by datasheet	

and skin effects on the AC resistance with different operating frequencies. The total AC loss can be obtained by summing up the separated losses at different frequencies based on the FFT analysis of the inductor current [22]. Level 2 thermal model using a resistance network to consider thermal resistances from the core to the winding, the core to ambient, and the winding to ambient is then adopted to verify the temperature of the inductors [23].

D. Capacitor Models

For the capacitor impedance modeling, a series *LRC* circuit is used with the ESL and ESR values provided by the database [24]-[25]. The thermal performance is also considered with the thermal resistance and the calculated RMS current loss.

V. CASE STUDY

With the design and optimization algorithms, and models discussed above. A comprehensive design can be implemented for the three-phase motor drive. This section presents an example of the design.

A. Design Specifications

Converter specifications are listed in TABLE III. For this specific case, the topology is selected as ANPC, the modulation used is continuous SVM, and the switching frequency selected is 60 kHz. The tool is used to optimize the device selection and passives design for the case.

TABLE III DESIGN SPECIFICATIONS

Design conditions	Source	1000V input with three wires input
	Load	Motor: $V_{LL-RMS}=673.6V$, $P=200\text{ kW}$, $f_0=1\text{ kHz}$
	Environment	$T_{amb}=40^\circ\text{C}$, liquid cooling for devices and forced air cooling for inductors
Design constraints	EMI	DO-160E for both DC and AC sides
	Harmonics	DO-160E
	Device Max. junction temperature	150°C
	Efficiency	>98%
	Design objective	Maximum specific power density

B. Design Results

The weight of the optimized converter is 11.34 kg (specific power density: 17.64 kW/kg). The efficiency is 98.7% (Total power loss: 2.5 kW). Detailed design results of components selection are listed in TABLE IV. The weight breakdown of the design is shown in Fig. 8.

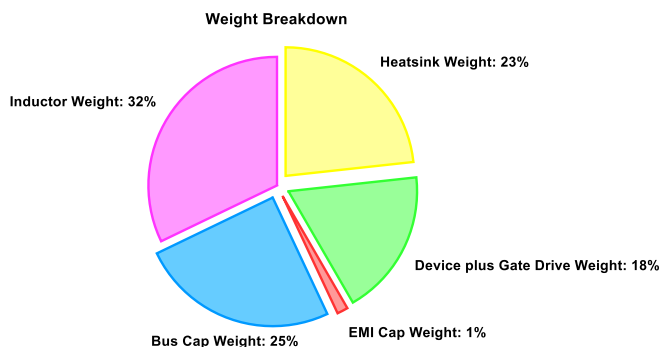


Fig. 8. Weight breakdown of the case study

TABLE IV DESIGN RESULTS

Device selection	High frequency switch	APTMC120AM09CT3AG (Microsemi, 1200 V, 220 A)
	Clamping switch	HT-3292-R-VB (Cree, 900 V, 664 A)
TMS	Cold plate	180-10-24C (Wakefield-vette)-
DC-link capacitors	Film capacitor	C4AEJBW5600A3NJ (KEMET, 60 μF , 10 parallel)
	CM inductor	176.7 μH (Core: Vitroperm 500FT60006-L2063-V110, winding: AWG0000, 3 turns)
DC side EMI filter	DM inductor	Leakage inductance of CM inductor: 0.93 μH
	CM capacitor	22 nF (B32022A3223M)
	DM capacitor	6.6 μF (3 parallel, BFC2 339 10225)
	CM inductor	1.97 mH (3 series, Core: Vitroperm 500FT60006-L2102-W468, winding: AWG00, 8 turns)
AC side EMI filter	DM inductor	Leakage inductance of CM inductor: 6.51 μH
	CM capacitor	23.5nF (2 series, B32022A3473M)
	DM capacitor	2.64 μF (8 parallel, R463I33300001M)
	CM inductor	1.97 mH (3 series, Core: Vitroperm 500FT60006-L2102-W468, winding: AWG00, 8 turns)

The advanced routine is selected for the case study. It takes around 3 hours to get the design results using a desktop computer with an Intel(R) Core(TM) i7-7700 CPU @ 3.60 GHz processor, 16 GB of RAM, and a 64-bit operating system. For the fast routine, it takes around 2 hours for the same case with the same desktop computer.

VI. SOFTWARE INTEGRATION: UI, DATABASE MANAGEMENT, AND RESULTS VISUALIZATION

A software integrating all design functions and models is developed in MATLAB App Designer with a user-friendly UI. Design conditions and constraints can be configured in the UI as shown in Fig. 9. The UI then recalls M-file functions with the configured design conditions and constraints to execute the selected models with the design algorithm to obtain the optimal design result. There are eight databases embedded in the software, which can be managed by users as shown in Fig. 10. Finally, the detailed design results including weight, loss, selected devices and passive components can be displayed as shown in Fig. 11. The results can also be visualized with pie and bar charts.

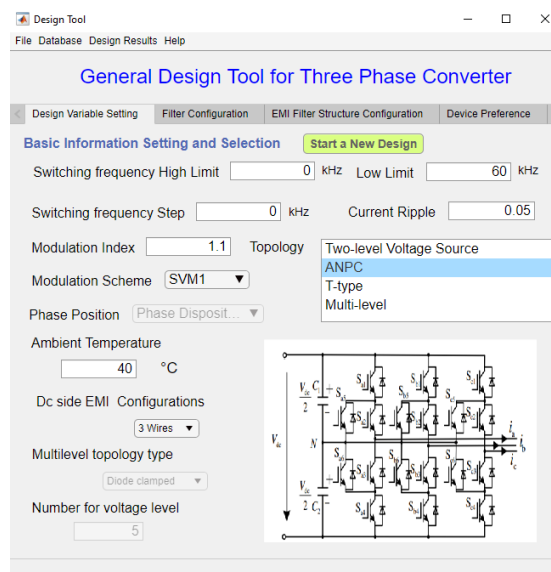


Fig. 9. UI for configuration

Part Num	Manufacturer	Historical	An (mm ²)	Cu (mm ²)	No (mm ²)	Wt (kg)		
1	VACUUMSCHMELZE	T60006-L2009-W114	Vitropem 500F	6	33.1821	26	190.1039	1.1000
2	VACUUMSCHMELZE	T60006-L2012-W1902	Vitropem 500F	7	59.2640	31	282.7350	1.7000
3	VACUUMSCHMELZE	T60006-L2012-W1498	Vitropem 500F	5	78.5375	35	220.8867	1.3000
4	VACUUMSCHMELZE	T60006-L2014-V0988	Vitropem 500F	4	102.0673	41	194.5217	1.1000
5	VACUUMSCHMELZE	T60006-L2015-W1055	Vitropem 500F	9	78.5375	39	441.7734	2.6000
6	VACUUMSCHMELZE	T60006-L2016-W1403	Vitropem 500F	14	78.5375	41	735.1110	4
7	VACUUMSCHMELZE	T60006-L2016-V1008	Vitropem 500F	14	78.5375	41	735.1110	4
8	VACUUMSCHMELZE	T60006-L2016-V1165	Vitropem 500F	14	78.5375	41	735.1110	4
9	VACUUMSCHMELZE	T60006-L2017-W1515	Vitropem 500F	12	124.6861	47	695.0098	4.1000
10	VACUUMSCHMELZE	T60006-L2018-V1184	Vitropem 500F	8	178.7094	53	534.9550	3.1000
11	VACUUMSCHMELZE	T60006-L2018-W1838	Vitropem 500F	16	178.7094	53	1.0681e+03	6.3000
12	VACUUMSCHMELZE	T60006-L2020-W1409	Vitropem 500F	24	122.7148	51	1.5319e+03	9
13	VACUUMSCHMELZE	T60006-L2020-W1450	Vitropem 500F	24	122.7148	51	1.5319e+03	9

Fig. 10. UI for database management

Design Results View

Design History: Design_Re ~ Switching Frequency: 60000 Hz Unit: Hz

Results Display:

- Switching Frequency: 60000 Hz
- Inductor Weight: 3.6466 kg
- Inductor Loss: 312.9669 W
- Capacitor Weight: 0.15487 kg
- Capacitor Loss: 2.3449 W
- Bus Cap Weight: 2.8175 kg
- Bus Cap Value: 277.7778 uF
- Device Weight: 2084.6 g
- Device Loss: 2216.5163 W
- Heat Sink Weight: 2.64 kg
- Total Weight: 11.3435 kg

Fig. 11. Design results visualization

VII. CONCLUSION

This paper presents a comprehensive design tool for the three-phase motor drive system. The design tool integrates state-of-the-art optimization algorithms and models to offer accurate design results as well as reduce paper design efforts for engineers. The converter is optimized for minimum weight by selecting design variables considering design constraints and conditions configured by users. The software is modular so that device and passive component models can be selected by users based on design speed and accuracy considerations. There are two design routines using different kinds of models. The fast routine utilizes simple analytical models while the advanced routine considers more non-linear physical characteristics of devices and passive components. The optimization algorithms and models utilized are presented in the paper. A case study with a 1 kV 200 kW three-phase motor drive is given. The UI, database management, and design results visualization are also presented.

ACKNOWLEDGMENT

This work made use of Engineering Research Center Shared Facilities supported by the Engineering Research Center Program of the National Science Foundation and the Department of Energy under NSF Award Number EEC-1041877 and the CURENT Industry Partnership Program.

REFERENCES

- [1] R. Lai *et al.*, "A systematic topology evaluation methodology for high-density three-phase PWM AC-AC converters," in *IEEE Transactions on Power Electronics*, vol. 23, no. 6, pp. 2665-2680, Nov. 2008.
- [2] F. Blaabjerg and J. K. Pedersen, "Optimized design of a complete three-phase PWM-VS inverter," in *IEEE Transactions on Power Electronics*, vol. 12, no. 3, pp. 567-577, May 1997.
- [3] H. Uemura, D. Yoshida, H. Fujimoto, Y. Okuma and J. W. Kolar, "Benefits and challenges of design process that employs a multi-objective optimization approach for industrial applications," *2015 IEEE 2nd International Future Energy Electronics Conference (IFEEC)*, Taipei, 2015, pp. 1-6.
- [4] H. Kragh, F. Blaabjerg and J. K. Pedersen, "An advanced tool for optimised design of power electronic circuits," *Conference Record of 1998 IEEE Industry Applications Conference. Thirty-Third IAS Annual Meeting*, St. Louis, MO, USA, 1998, pp. 991-998 vol.2.
- [5] I. Laird, X. Yuan, J. Scoltock and A. Forsyth, "A Design Optimisation Tool for Maximising the Power Density of 3-Phase DC-AC Converters Using Silicon Carbide (SiC) Devices," in *IEEE Transactions on Power Electronics*, vol. PP, no. 99, pp. 1-1.
- [6] F. Wang, W. Shen, D. Boroyevich, S. Ragon, V. Stefanovic and M. Arpilliere, "Design Optimization of Industrial Motor Drive Power Stage Using Genetic Algorithms," *2006 CES/IEEE 5th International Power Electronics and Motion Control Conference*, Shanghai, 2006, pp. 1-5.
- [7] PowerForge software, available online: <https://www.powerdesign.tech/>.
- [8] F. Wang, W. Shen, D. Boroyevich, S. Ragon, V. Stefanovic, and M. Arpilliere, "Voltage Source Inverter - Development of a design optimization tool", *IEEE Industry Applications Magazine*, Volume 15, Issue 2, March-April 2009 pp. 24 - 33
- [9] J. Kennedy and R. C. Eberhart, "Particle swarm optimization," in *Proc. IEEE Int. Conf. Neural Netw.*, Perth, Australia, Nov. 27-Dec. 1, 1995, pp. 1942-1948
- [10] Marouchos, Christos C. *The switching function: analysis of power electronic circuits*. Vol. 17. IET, 2006.
- [11] D. Han, S. Li, Y. Wu, W. Choi, and B. Sarlioglu, "Comparative analysis on conducted CM EMI Emission of motor drives: WBG versus Si devices," *IEEE Transactions on Industrial Electronics*, vol. 64, no. 10, pp. 8353-8363, 2017.
- [12] R. Ren, Z. Dong, and F. F. Wang, "Bridging gaps in paper design considering impacts of switching speed and power-loop layout," in *2020 IEEE Energy Conversion Congress and Exposition (ECCE)*, pp. 1992-1999.
- [13] M. Kamon, M. J. Tsuk, and J. K. White, "FASTHENRY: A multipole-accelerated 3-D inductance extraction program," *IEEE Transactions on Microwave theory and techniques*, vol. 42, no. 9, pp. 1750-1758, 1994.
- [14] AAVID, "AAVID product selection guide," ed, 2010.
- [15] P. Ning, F. F. Wang, and K. D. Ngo, "Forced-air cooling system design under weight constraint for high-temperature SiC converter," *IEEE Transactions on Power Electronics*, vol. 29, no. 4, pp. 1998-2007, 2013.
- [16] M. K. Kazimierczuk, *High-frequency magnetic components*. John Wiley & Sons, 2009.
- [17] Z. Dong, R. Ren, B. Liu, and F. Wang, "Data-driven leakage inductance modeling of common mode chokes," in *2019 IEEE Energy Conversion Congress and Exposition (ECCE)*, pp. 6641-6646.
- [18] R. Ren, Z. Dong, B. Liu, and F. Wang, "Leakage inductance estimation of toroidal common-mode choke from perspective of analogy between reluctances and capacitances," in *2020 IEEE Applied Power Electronics Conference and Exposition (APEC)*, pp. 2822-2828.
- [19] R. Ren, B. Liu, Z. Dong, and F. Wang, "Current-bias dependent permeability of powder and amorphous core induced unbalanced DM impedance and mixed-mode noise," in *2019 IEEE Energy Conversion Congress and Exposition (ECCE)*, pp. 2873-2880.
- [20] R. Ren, Z. Dong, B. Liu, and F. Wang, "Impedance-based common-mode inductor design approach considering frequency-dependent and imaginary permeability," in *2020 IEEE Applied Power Electronics Conference and Exposition (APEC)*, pp. 2680-2686.
- [21] K. Venkatachalam, C. R. Sullivan, T. Abdallah, and H. Tacca, "Accurate prediction of ferrite core loss with nonsinusoidal waveforms using only Steinmetz parameters," in *2002 IEEE Workshop on Computers in Power Electronics*, pp. 36-41.
- [22] E. Bennett and S. C. Larson, "Effective resistance to alternating currents of multilayer windings," *Electrical Engineering*, vol. 59, no. 12, pp. 1010-1016, 1940.
- [23] C. W. T. McLyman, *Transformer and inductor design handbook*. CRC press, 2016.
- [24] L. Jun and O. Lorentz, "Modeling ceramic and tantalum capacitors by automatic SPICE parameter extractions," in *Twentieth Annual IEEE Applied Power Electronics Conference and Exposition*, 2005.
- [25] T. Epcos, "Film capacitors, general technical information," ed, 2018.